Kruglov, I. A., Kvashnin, A. G., Goncharov, A. F., Oganov, A. R., Lobanov, S. S., Holtgrewe, N., Jiang, S., Prakapenka, V. B., Greenberg, E., Yanilkin, A. V. (2018): Uranium polyhydrides at moderate pressures: Prediction, synthesis, and expected superconductivity. - *Science Advances*, *4*, 10.

DOI: http://doi.org/10.1126/sciadv.aat9776

CHEMISTRY

Uranium polyhydrides at moderate pressures: Prediction, synthesis, and expected superconductivity

Ivan A. Kruglov[1,2]*, Alexander G. Kvashnin[3,2], Alexander F. Goncharov[4,5]*, Artem R. Oganov[1,2,3]*, Sergey S. Lobanov[5,6], Nicholas Holtgrewe[5,7], Shuqing Jiang[4], Vitali B. Prakapenka[7], Eran Greenberg[7], Alexey V. Yanilkin[1,2]

Hydrogen-rich hydrides attract great attention due to recent theoretical (*1*) and then experimental discovery of record high-temperature superconductivity in H_3S [T_c = 203 K at 155 GPa (*2*)]. Here we search for stable uranium hydrides at pressures up to 500 GPa using ab initio evolutionary crystal structure prediction. Chemistry of the U-H system turned out to be extremely rich, with 14 new compounds, including hydrogen-rich UH_5, UH_6, U_2H_{13}, UH_7, UH_8, U_2H_{17}, and UH_9. Their crystal structures are based on either common face-centered cubic or hexagonal close-packed uranium sublattice and unusual H_8 cubic clusters. Our high-pressure experiments at 1 to 103 GPa confirm the predicted UH_7, UH_8, and three different phases of UH_5, raising confidence about predictions of the other phases. Many of the newly predicted phases are expected to be high-temperature superconductors. The highest-T_c superconductor is UH_7, predicted to be thermodynamically stable at pressures above 22 GPa (with T_c = 44 to 54 K), and this phase remains dynamically stable upon decompression to zero pressure (where it has T_c = 57 to 66 K).

INTRODUCTION

Uranium hydride is a highly toxic compound that spontaneously ignites in the air (*3*) and reacts with water (*4*). It is used mainly for separation of hydrogen isotopes (*5*), but it can also be a component of explosives. It was first synthesized by F. Driggs during heating of metallic uranium in hydrogen atmosphere, and it was initially the assigned the composition UH_4. Later, the composition was determined as UH_3 (*6*): this phase is known as β-UH_3. When bulk uranium was heated in hydrogen atmosphere at lower temperature (*7*), a metastable α-UH_3 phase appeared, and transformation to β-UH_3 occurred above 523 K. The crystal structure of α-UH_3 is of Cr_3Si-type (also known as A15 or β-W); U atoms have icosahedral coordination and form a body-centered cubic sublattice. Many superconductors belong to the Cr_3Si structure type (for example, Nb_3Sn). The structure of β-UH_3 is more complex and based on a β-W–like uranium sublattice containing hydrogen atoms in distorted tetrahedral voids (*8*, *9*). UH_3 is the only known uranium hydride found to be stable at ambient conditions [although there is evidence of isolated molecules of UH, UH_2, UH_4, UH_3, U_2H_2, and U_2H_4 (*10*)]. Hydrogen, being a molecular solid, has large atomic volume in the elemental form—volume reduction, favorable under pressure, can be achieved through compound formation, and one expects polyhydrides to form under pressure. Another motivation was that some uranium compounds were shown to have peculiar (and previously inconceivable) coexistence of superconductivity and ferromagnetism (*11*–*13*), and (nonmagnetic) polyhydrides are prime candidates for high-temperature superconductivity.

RESULTS AND DISCUSSION

To predict stable phases in the U-H system at pressures of 0, 5, 25, 50, 100, 200, 300, 400, and 500 GPa, we performed variable-composition evolutionary structure/compound searches using the Universal Structure Predictor: Evolutionary Xtallography (USPEX) algorithm (*14*–*16*). By definition, a thermodynamically stable phase has lower Gibbs free energy (or, at 0 K, lower enthalpy) than any phase or phase assemblage of the same composition. Having predicted stable compounds and their structures at different pressures (Fig. 1), we built the composition-pressure phase diagram (Fig. 2), which shows pressure ranges of stability (with an estimated numerical error of approximately 1 to 2 GPa) for all the phases found (for convex hull diagrams at the selected pressures, see fig. S1). As shown in Fig. 2, our calculations correctly reproduce stability of both phases of UH_3 and predict 12 new stable phases corresponding to 14 new compounds (*Cmcm*-UH and $P6_3/mmc$-UH, *Ibam*-U_2H_3, *Pbcm*-UH_2, *C*2/*c*-U_2H_5, α-UH_3 and β-UH_3, *Immm*-U_3H_{10}, $P6_3mc$-UH_5, $P6_3/mmc$-UH_6, $P\bar{6}m2$-U_2H_{13}, $P6_3/mmc$-UH_7, $Fm\bar{3}m$-UH_8, $P\bar{4}m2$-U_2H_{17}, $P6_3/mmc$-UH_9, and metastable $F\bar{4}3m$-UH_9). Detailed information on crystal structures of the predicted phases can be found in table S1 and fig. S2. Phonon calculations confirmed that none of the newly predicted phases have imaginary phonon frequencies in their predicted ranges of thermodynamic stability

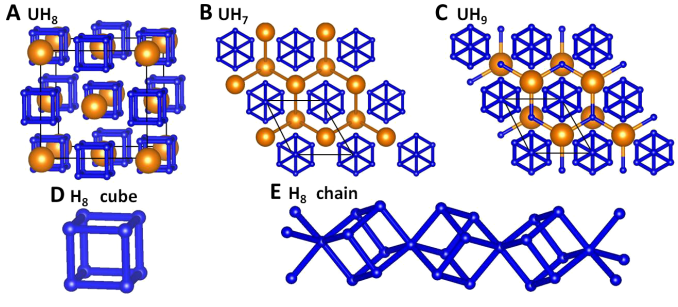

Fig. 1. Crystal structures of the predicted phases. (**A**) $Fm\bar{3}m$-UH_8, (**B**) $P6_3/mmc$-UH_7, and (**C**) $P6_3/mmc$-UH_9. (**D** and **E**) Basic hydrogen motifs. U atoms are shown by large orange balls, and hydrogens are shown by small blue balls.

[1]Dukhov Research Institute of Automatics (VNIIA), Moscow 127055, Russian Federation. [2]Moscow Institute of Physics and Technology, Dolgoprudny, Moscow Region 141700, Russian Federation. [3]Skolkovo Institute of Science and Technology, 3 Nobel St., Moscow 143026, Russian Federation. [4]Key Laboratory of Materials Physics, Institute of Solid State Physics CAS, Hefei 230031, China. [5]Geophysical Laboratory, Carnegie Institution of Washington, Washington, DC 20015, USA. [6]GFZ German Research Center for Geosciences, Section 4.3, Telegrafenberg, 14473 Potsdam, Germany. [7]Center for Advanced Radiations Sources, University of Chicago, Chicago, IL 60637, USA.
*Corresponding author. Email: ivan.kruglov@phystech.edu (I.A.K.); a.oganov@skoltech.ru (A.R.O.); agoncharov@carnegiescience.edu (A.F.G.)

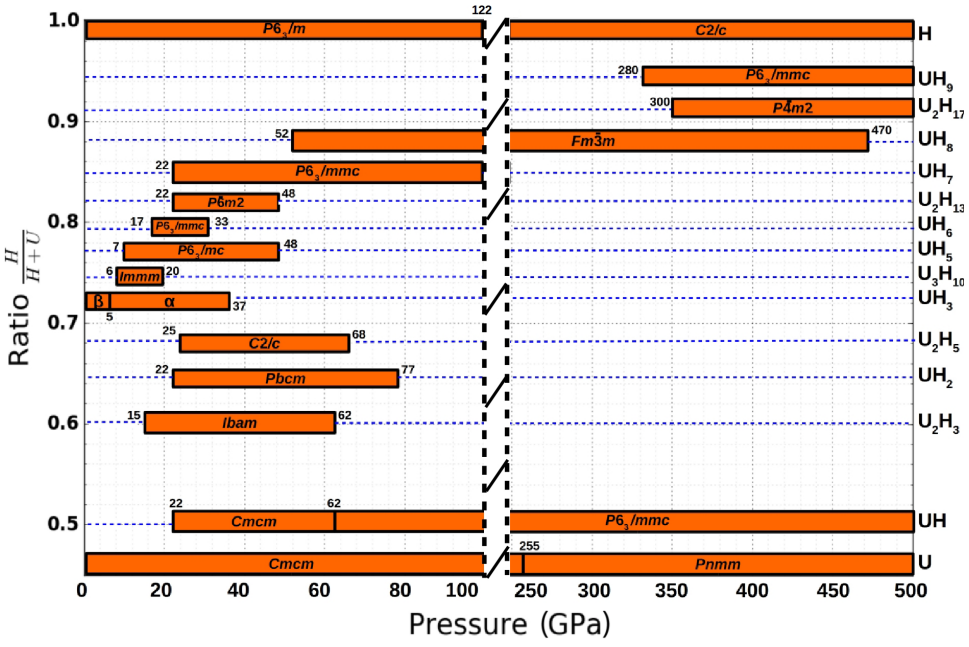

Fig. 2. Pressure-composition phase diagram of the U-H system.

(see phonon dispersion curves and densities of states in the supplementary materials). The only uranium hydride phase remains stable at zero pressure is β-UH_3, which transforms into α-phase above 5.5 GPa (fig. S3).

Among the numerous predicted stable U-H phases, below, we focus on hydrogen-rich (H/U > 3) polyhydrides as potential high-temperature superconductors. All these hydrogen-rich phases are metallic, and their crystal structures feature very notable building blocks—H_8 cubes (Fig. 1, D and E). Lattice dynamics calculations show a big gap between phonon contributions from uranium and hydrogen atoms due to their large mass difference: Low-frequency modes mostly belong to uranium atoms, while high-frequency modes belong to hydrogen (fig. S4).

The first hydrogen-rich compound, U_3H_{10}, is predicted to become stable at 6 GPa. This structure is a derivative of α-UH_3 with one additional hydrogen atom and a tripled lattice parameter along the *c* direction. At pressures above 7 GPa, a family of UH_{5-7} hydrides becomes stable with the same hexagonal close-packed (hcp) sublattice of U atoms. The $P6_3/mmc$-UH_7 structure (Fig. 1B) is a derivative of the anti-NiAs structure, where all octahedral voids of U sublattice are filled by H_8 cubes (occupying the same positions as nickel atoms in the NiAs structure), forming infinite one-dimensional (1D) chains that run along the *c* axis, with each H_8 cube sharing a corner with neighboring two cubes in the chain (Fig. 1E). At 20 GPa, the shortest H-H distance is 1.56 Å, and the U-H distances vary from 2.12 to 2.25 Å. $P\bar{6}m2$-U_2H_{13} is a derivative of the UH_7 structure, with a doubled unit cell along the *c* direction: U atoms still form an hcp sublattice, but half of linkages between H_8 cubes are deleted. As a result, instead of infinite 1D chains of corner-sharing H_8 cubes, we have isolated ("0D") corner-sharing pairs of incomplete H_7 cubes and the composition changes from $UH_7 = U_2H_{14}$ to $U_2H_{14-1} = U_2H_{13}$. At 20 GPa, the H-H distance is 1.55 Å, and the U-H distances vary from 2.09 to 2.13 Å. Derivatives of U_2H_{13}, the UH_6 and UH_5 structures, form after deletion of corner-sharing H atoms in the pair of H_7-cubes and another hydrogen atom from the chain, respectively. Evolution of the hydrogen chains in the octahedral channels is presented in Fig. 3. The only magnetic phase among UH_{5-7} hydrides is UH_5 (fig. S4). Notably, lattice dynamics calculations indicate that all these phases are dynamically stable even at zero pressure, that is, they may exist as metastable materials at atmospheric pressure (fig. S5).

At a higher pressure of 52 GPa, a new stable hydrogen-rich phase is predicted—UH_8 (Fig. 1A). At pressures between 100 and 280 GPa, UH_8 is the only stable hydrogen-rich uranium hydride. Its structure is a derivative of the rocksalt structure, where U atoms occupy Na sites and isolated H_8 cubes occupy Cl sites. At 50 GPa, the H-H distances are 1.38 Å and the U-H distances are 2.13 Å. The coordination number of uranium atoms in this remarkable structure is equal to 24. At 280 GPa, another stable compound appears—UH_9 (Fig. 1C). It is structurally similar to UH_7: Just like UH_7, it has an hcp sublattice of uranium atoms and infinite 1D chains of corner-sharing H_8 cubes running along the *c* axis, but in addition, it has single H atoms located within close-packed uranium layers (Fig. 1C). At 300 GPa, the shortest H-H distances are 1.13 Å within H_8 cubes and 1.09 and 1.23 Å between the cubes. Besides the above-mentioned stable phase of UH_9, our calculations uncovered a low-enthalpy metastable (by only 18 meV/atom) polymorph with a space group $F\bar{4}3m$. This metastable structure (fig. S2J) is based on the face-centered cubic (fcc) sublattice of uranium atoms, all the octahedral voids of which are occupied by isolated H_8 cubes, and half of the tetrahedral voids are occupied by single H atoms. This structure can be described as a half-Heusler alloy. USPEX found a stable U_2H_{17} (fig. S2I) whose structure is a derivative of the cubic UH_9, with half of single H atom positions vacant in the alternating layer, which lowers symmetry to tetragonal $P\bar{4}$m2.

We have successfully synthesized the predicted uranium hydrides in a diamond anvil cell (DAC) at various pressures (1 to 103 GPa) on loading and unloading cycles, applying moderate laser heating (up to 2000 K) in the loading cycles. Three experiments examined the reaction pathways of U and H_2. In one control experiment, U was loaded in Ar medium, and in the other two, naturally oxidized uranium samples were studied in H_2 medium (these latter ones will not

be considered here). Experiments with the Ar medium revealed the presence of metallic U and a small amount (<5%) of fcc UO_2 [for example, ref. (*17*)]. In the experiments with H_2 medium, UO_2 was not detected. Shortly after H_2 loading to an initial pressure (0.1 to 2 GPa), the U sample swells and changes appearance, and x-ray diffraction (XRD) shows the formation of coexisting α-UH_3 and β-UH_3 (Fig. 4A). At the lowest pressures, the amount of α-UH_3 is approximately 30%. As the pressure increases, the share dwindles until this phase becomes undetectable above 5 GPa (or 7.5 GPa if not heated).

In contrast, β-UH_3 remains metastable up to 69 GPa (if not heated). The experimental unit cell volumes of these UH_3 phases are slightly larger (within 3%) compared to our theoretical predictions (Fig. 5). Above 5 GPa, a new phase starts to appear after laser heating. It becomes a dominant phase at 8 GPa (Fig. 4B) and remains detectable at up to 36 GPa. It is fcc-based, and the hydrogen content can be evaluated using the measured and calculated unit cell volumes (Fig. 5). If we assume $x = 5$, the experimental volumes are again slightly larger than the theoretically calculated ones. Other predicted UH_5 structures

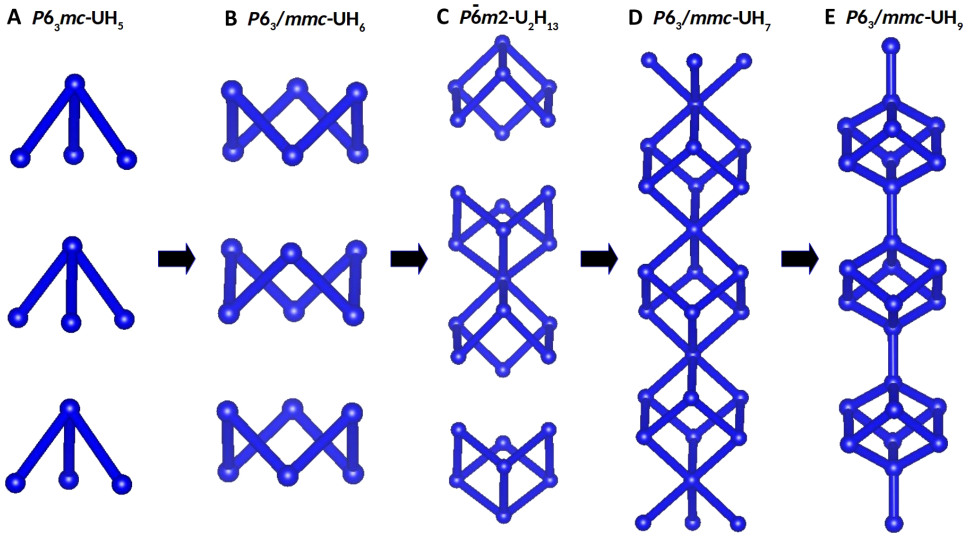

Fig. 3. Evolution of hydrogen sublattice in hcp UH_{5-7} structures.

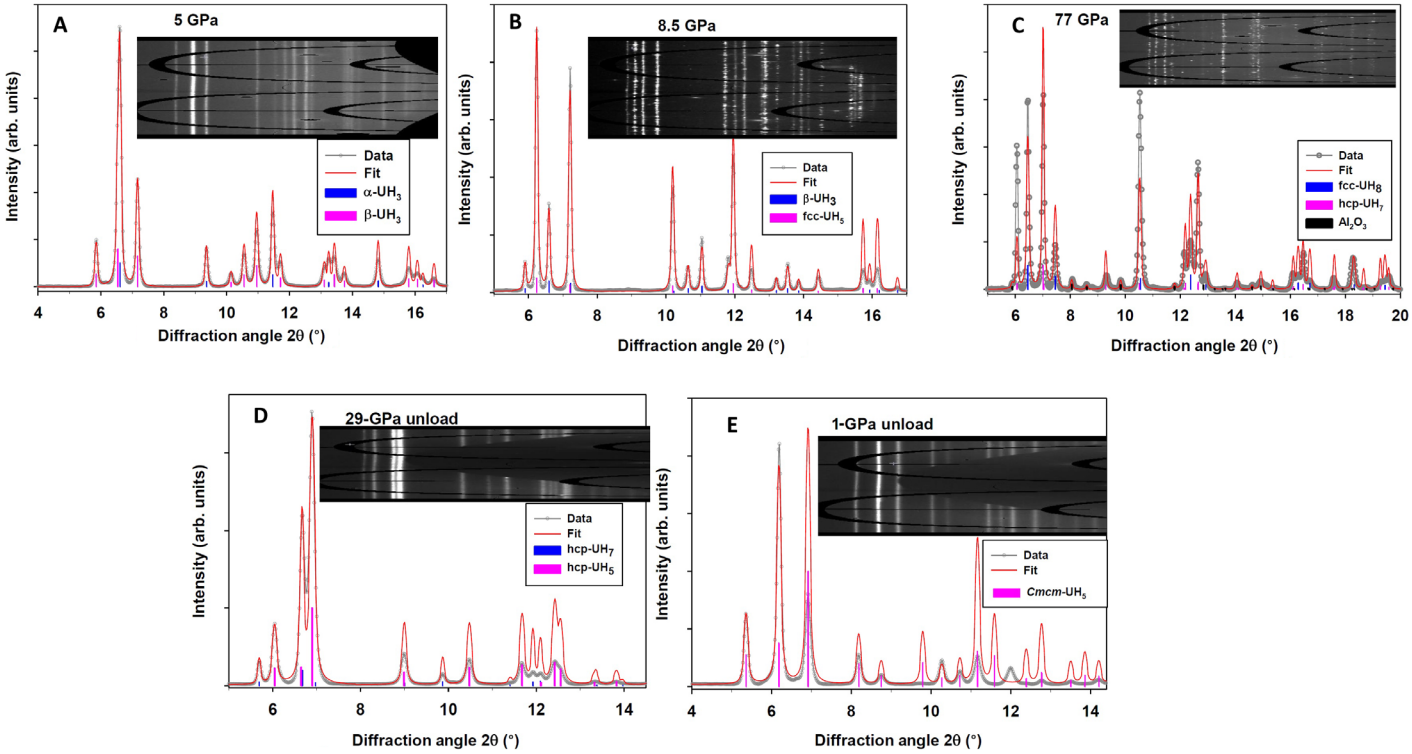

Fig. 4. Experimental data on U-H compounds. XRD patterns of synthesized U-H phases: α-UH_3 and β-UH_3 (**A**), fcc UH_5 (**B**), hcp UH_7 and fcc $UH_{8+\delta}$ (**C**), hcp UH_5 (**D**), and *Cmcm*-UH_5 (**E**).

(with very similar volumes) are hcp-like and orthorhombic, and these will be discussed below. The structure of fcc UH_5 is similar to the predicted UH_8, but instead of H_8 cubes, it has alternating H_4 tetrahedra and single H atoms (fig. S6B). At 31 GPa, another hydride starts to appear; it matches well with the predicted hcp UH_7 phase. This polyhydride can be observed at up to 103 GPa, which is the highest pressure in this study, and can be present as a single phase. However, above 45 GPa, weak peaks of yet another fcc structure appear (Fig. 4C), which remains stable up to 103 GPa. Volume of this phase is close to the theoretically found $F\bar{4}3m$-UH_9 structure (metastable above 280 GPa) (see Fig. 5), but its formation pressure is close to the UH_8 phase (52 GPa). Thus, we believe that this experimental phase is an intermediate structure between fcc UH_8 and UH_9 phases, and later in the text, we will denote it as $UH_{8+\delta}$.

We also looked at potential metastability of phases synthesized under extreme conditions and also at possible appearance of some other metastable phases, which can be realized because of kinetic reasons. No laser heating was applied in unloading cycles from 60, 45, and 38 GPa. A uniquely identified hexagonal UH_7 phase remains metastable down to at least 29 GPa. At this pressure, we could have been able to identify a hexagonal UH_5 phase which was theoretically predicted (Fig. 4D). However, at lower pressure, the diffraction patterns become very complex, possibly representing a mixture of several phases that could not be uniquely identified and also remnants of unreacted β-UH_3. After unloading under nearly-ambient conditions (near 1 GPa), a single phase appeared to have been formed, which we were able to index in an orthorhombic lattice with a = 3.438 Å, b = 7.15 Å, and c = 6.20 Å and the space group *Cmma* (Fig. 4E). The unit cell volume suggests the UH_5 composition (Fig. 5), although UH_4 could also be possible. The best match from among the theoretically predicted structures is *Cmcm*-UH_5, which is above the convex hull by 5 meV/atom at 5 GPa. This structure describes well most of the observed peaks, although there

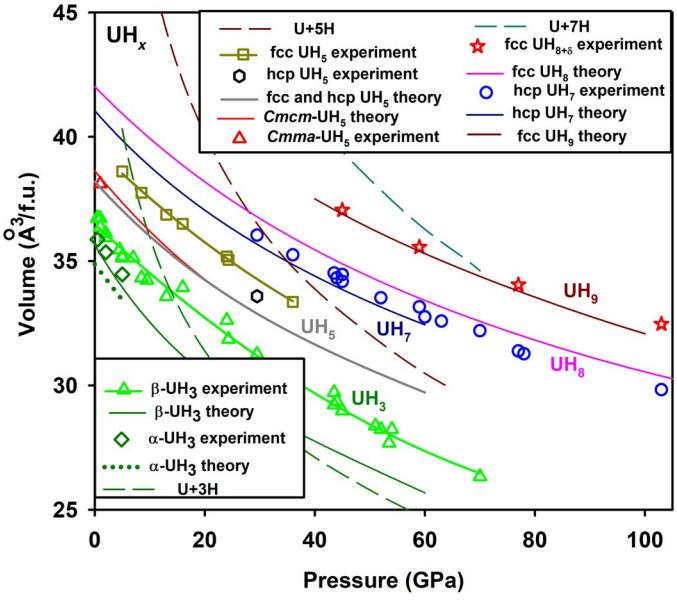

Fig. 5. Volumes per formula unit as a function of pressure for the polyhydrides synthesized in this work in comparison to theoretical predictions. The combined literature volumes of U metal and solid molecular hcp H_2 in different proportions are also shown to illustrate the stability of polyhydrides at high pressures. f.u., formula unit.

are some discrepancies too (Fig. 4E). The volume-pressure data for the newly synthesized α-UH_3 and β-UH_3, orthorhombic UH_5, hcp UH_5 and UH_7, and fcc UH_5 and UH_8 are compared in Fig. 5 to the calculations and combinations of the experimental equations of state of hcp H_2 and metallic U (*18*). The latter comparison shows that the polyhydrides are stable when their volumes are lower than the sum of volumes of the elements. As one can see in Fig. 5, the polyhydrides with higher H content require higher pressures for their stability; this trend emerges both from our experiments and structure predictions. More detailed XRD patterns can be found in figs. S7 to S11.

The calculated electronic band structures of the predicted stable U-H phases are shown in fig. S4. All these phases are metallic and feature numerous flat bands near the Fermi level. Only UH_3 and UH_5 phases are magnetic (below 100 and 170 GPa, respectively). Their ferromagnetism can also be seen from the band structures shown in fig. S4 (A to C), where contributions of U atoms to the spin-up and spin-down states are shown in red and blue, respectively.

While for UH_3, the bands near the Fermi level come mainly from uranium orbitals, in uranium polyhydrides, contributions of both uranium and hydrogen atoms are large. Geometric similarities (for example, between $P6_3/mmc$-UH_7 and $P\bar{6}m2$-U_2H_{13}) result in similar densities of states and electronic properties (see fig. S4, E and F). Likewise, stable $P6_3/mmc$ and metastable $F\bar{4}3m$ polymorphs of UH_9 (actually, these can even be described as polytypes) have similar electronic density of states due to geometric similarities of their crystal structures. As we will see below, similarities are observed also for electron-phonon coupling (EPC) coefficients and superconducting T_c.

In the Migdal-Eliashberg theory of superconductivity, the central quantity is the EPC coefficient λ. The superconducting transition temperature (T_c) can be calculated using the Allen-Dynes–modified McMillan formula (Eq. 1) or directly solving the Eliashberg equation (for details, see Materials and methods and supplementary materials), where for the Coulomb pseudopotential μ*, we use the commonly accepted bracketing values of 0.10 and 0.15. All T_c values were calculated using the Eliashberg equation (which is more accurate by definition), but the critical temperature values calculated using the Allen-Dynes–modified McMillan formula (table S2) are in agreement with the data presented below. Detailed information on the calculated superconducting properties of uranium hydrides is given in Table 1, and spectral function $\alpha^2F(\omega)$ and the integrated EPC coefficient λ for

Table 1. Predicted superconducting properties of uranium hydrides. Two T_c values were calculated by solving the Eliashberg equation with μ* equal to 0.1 and 0.15, respectively.

Phase	Space group	Pressure (GPa)	ω_{log} (K)	λ	T_c (K)
UH_7	$P6_3/mmc$	20	873.8	0.83	54.1 43.7
		0	764.9	0.95	65.8 56.7
UH_8	$Fm\bar{3}m$	50	873.7	0.73	33.3 23.4
		0	450.3	1.13	55.2 46.2
UH_9	$P6_3/mmc$	300	933.4	0.67	31.2 19.9

UH_{7-9} are presented on fig. S12. For UH_7 at 20 GPa, we find an EPC coefficient of 0.83 resulting in T_c in the range of 44 to 54 K (57 to 66 K at 0 GPa; see Table 1). The structurally related U_2H_{13} should display similar EPC coefficient and T_c values. For UH_8 at 50 GPa, we predict $\lambda = 0.73$ and T_c in the range of 23 to 33 K (46 to 55 K at 0 GPa). $P6_3/mmc$-UH_9 at 300 GPa has the lowest T_c among the above considered hydrides (20 to 31 K at 300 GPa).

CONCLUSIONS

In summary, using the evolutionary crystal structure prediction algorithm USPEX, we found 14 new uranium hydrides, including hydrogen-rich, high-temperature superconductors UH_7, UH_8, UH_9, U_2H_{13}, and U_2H_{17}. Their crystal structures are based on either fcc or hcp uranium sublattice and H_8 cubic clusters. Our high-pressure experiments have successfully produced UH_5 at the pressure of 5 GPa, UH_7 at 31 GPa, and $UH_{8+\delta}$ at 45 GPa, corroborating our predictions and confirming their reliability. New uranium hydrides have been identified by close match of theoretically calculated and experimental XRD patterns and equations of state. We predict UH_{7-9} to be superconductors with maximum T_c for UH_7 (54 K at 20 GPa). Superconducting uranium hydrides appear at unusually low pressures. Given dynamical stability of UH_{7-8} at zero pressure, there is a possibility for them to exist as metastable phases at ambient pressure where their T_c values will reach 57 to 66 K. Furthermore, given the presence of a pseudogap at the Fermi level for all UH_{7-9} compounds, we expect doping to be effective in raising T_c. This and other works [Ac-H (*19*) and Th-H (*20*)] bring the possibility of new high-temperature superconductors based on actinides. Present work shows the predictive power of modern methods of crystal structure prediction capable of finding unusual materials with exotic chemistry.

MATERIALS AND METHODS

Similar methodology was used in ref. (*19*).

Theoretical calculations

The evolutionary algorithm USPEX (*14*–*16*) is a powerful tool for predicting thermodynamically stable compounds of given elements at a given pressure. We performed variable-composition searches in the U-H system at 0, 5, 25, 50, 100, 200, 300, 400, and 500 GPa. The first generation (120 structures) was created using a random symmetric generator, while all subsequent generations contained 20% of random structures, and 80% of structures created using heredity, soft mutation, and transmutation operators. Within USPEX runs, structure relaxations were performed at the generalized gradient approximation level [with the functional from ref. (*21*)] of density functional theory using the projector-augmented wave method (*22*) as implemented in the Vienna Ab initio Simulation Package (VASP) code (*23*–*25*). Plane-wave kinetic energy cutoff was set to 600 eV, and the Brillouin zone was sampled by the Γ-centered *k*-mesh with a resolution of $2\pi \times 0.05$ Å^{-1}.

To establish stability fields of the predicted phases, we recalculated their enthalpies with increased precision at various pressures with a smaller pressure increment (from 1 to 10 GPa), recalculating the thermodynamic convex hull at each pressure. The phases that were located on the convex hull are the ones stable at given pressure. Stable structures of elemental H and U were taken from USPEX calculations and from (*26*) and (*27*), respectively.

The superconducting properties were calculated using the QUANTUM ESPRESSO (QE) package (*28*). The phonon frequencies and EPC coefficients were computed using density-functional perturbation theory (*29*) using the plane-wave pseudopotential method and Perdew-Burke-Ernzerhof exchange correlation functional (*21*). Convergence tests showed that 60 rydberg (Ry) is a suitable kinetic energy cutoff for the plane-wave basis set. Electronic band structures of UH_7 and UH_8 were calculated using both VASP and QE and demonstrated good consistency. Comparison of the phonon densities of states calculated using the finite displacement method [VASP and PHONOPY (*30*)] and density-functional perturbation theory (QE) showed perfect agreement between these methods.

Critical temperature was calculated from the Eliashberg equation (*31*), which is based on the Fröhlich Hamiltonian $\hat{H} = \hat{H}_e + \hat{H}_{ph} + \sum_{k,q,j} g^{q,j}_{k+q,k} \hat{c}^+_{k+q} \hat{c}_k (\hat{b}^+_{-q,j} + \hat{b}_{q,j})$ where c^+ and b^+ relate to creation operators of electrons and phonons, respectively. The matrix element of electron-phonon interaction $g^{q,j}_{k+q,k}$ calculated within the harmonic approximation in QE can be defined as $g^{q,j}_{k+q,k} = \sqrt{\frac{\hbar}{2M\omega_{q,j}}} \int \psi^*_k(r) \cdot \left\{ \frac{dV_{scf}}{d\vec{u}_q} \cdot \frac{\vec{u}_q}{|\vec{u}_q|} \right\} \cdot \psi_{k+q}(r) d^3r$, where u_q is the displacement of an atom with mass M in the phonon mode q,j. Within the framework of Gor'kov (*32*) and Migdal (*33*) approach, the correction to the electron Green's function $\Sigma(\vec{k}, \omega) = G_0^{-1}(\vec{k}, \omega) - G^{-1}(\vec{k}, \omega)$ caused by interaction can be calculated by taking into account only the first terms of the expansion of electron-phonon interaction in series of (ω_{log}/E_F). As a result, it will lead to integral Eliashberg equations (*31*). These equations can be solved using an iterative self-consistent method for the real part of the order parameter $\Delta(T, \omega)$ (superconducting gap) and the mass renormalization function $Z(T, \omega)$ (for more details, see the supplementary materials) (*34*).

In our calculations of the EPC parameter λ, the first Brillouin zone was sampled using a 2 by 2 by 2 *q*-points mesh and a denser 24 by 24 by 24 *k*-points mesh (with Gaussian smearing and $\sigma = 0.03$ Ry, which approximates the zero-width limits in the calculation of λ). The superconducting transition temperature T_c was also estimated using the Allen-Dynes–modified McMillan equation (*35*).

$$T_C = \frac{\omega_{log}}{1.2} \exp\left(\frac{-1.04(1+\lambda)}{\lambda - \mu^*(1+0.62\lambda)} \right) \quad (1)$$

where ω_{log} is the logarithmic average frequency, and μ* is the Coulomb pseudopotential for which we used widely accepted lower and upper bound values of 0.10 and 0.15. The EPC constant λ and ω_{log} were calculated as

$$\lambda = 2\int_0^\infty \frac{\alpha^2 F(\omega)}{\omega} d\omega \quad (2)$$

and

$$\omega_{log} = \exp\left(\frac{2}{\lambda} \int \frac{d\omega}{\omega} \alpha^2 F(\omega) ln(\omega) \right) \quad (3)$$

Experiments

We performed experiments in laser-heated DACs with 200- to 300-μm central culets. Small pieces of uranium metal (with naturally oxidized surfaces) were thinned down to 5 to 8 μm and mechanically or laser-cut

to 40 to 60 linear dimensions. These were positioned in a hole in a rhenium gasket that was filled with H_2 gas at ≈150 MPa along with small Au chips for pressure measurements. In a control experiment, the sample cavity was filled by Ar gas. The loaded material was successively laser heated to 1700 K at various pressures during sample loading using microsecond-long pulses of a 1064-nm Yb-doped yttrium aluminum garnet fiber laser (*36*). We used this pulsed laser heating mode to avoid premature diamond breakage, which is common with DAC loaded with hydrogen. Synchrotron XRD measurements (x-ray wavelength of 0.3344 Å) at GeoSoilEnviroCARS (GSECARS), Advanced Photon Source (APS), Argonne National Laboratory (ANL) (*37*), and an x-ray beam spot as small as 3 μm by 4 μm were used to probe the physical and chemical state of the sample.

SUPPLEMENTARY MATERIALS

Supplementary material for this article is available at http://advances.sciencemag.org/cgi/content/full/4/10/eaat9776/DC1

Fig. S1. Convex hull diagrams for UH_3 and UH_{5-9}.
Fig. S2. Crystal structures of the predicted U-H phases.
Fig. S3. Enthalpy difference between β-UH_3 and α-UH_3.
Fig. S4. Electronic band structures of predicted uranium hydrides.
Fig. S5. Phonon band structures and densities of states of predicted uranium hydrides.
Fig. S6. Crystal structures of the experimentally found UH_5 structures.
Fig. S7. Experimental data on U-H compounds: XRD pattern at 5 GPa.
Fig. S8. Experimental data on U-H compounds: XRD pattern at 8.5 GPa.
Fig. S9. Experimental data on U-H compounds: XRD pattern at 77 GPa.
Fig. S10. Experimental data on U-H compounds: XRD pattern at 29 GPa (unloading).
Fig. S11. Experimental data on U-H compounds: XRD pattern at 1 GPa (unloading).
Fig. S12. Spectral function $\alpha^2F(\omega)$ and EPC coefficient $\lambda(\omega)$ for different uranium hydrides.
Table S1. Crystal structures of predicted uranium hydrides.
Table S2. Predicted superconducting properties of uranium hydrides from the Allen-Dynes–modified McMillan formula.
References (*38*–*40*)

REFERENCES AND NOTES

1. D. Duan, Y. Liu, F. Tian, D. Li, X. Huang, Z. Zhao, H. Yu, B. Liu, W. Tian, T. Cui, Pressure-induced metallization of dense $(H_2S)_2H_2$ with high-T_c superconductivity. *Sci. Rep.* **4**, 6968 (2015).
2. A. P. Drozdov, M. I. Eremets, I. A. Troyan, V. Ksenofontov, S. I. Shylin, Conventional superconductivity at 203 kelvin at high pressures in the sulfur hydride system. *Nature* **525**, 73–76 (2015).
3. F. Le Guyadec, X. Génin, J. P. Bayle, O. Dugne, A. Duhart-Barone, C. Ablitzer, Pyrophoric behaviour of uranium hydride and uranium powders. *J. Nucl. Mater.* **396**, 294–302 (2010).
4. R. Orr, H. Godfrey, C. Broan, D. Goddard, G. Woodhouse, P. Durham, A. Diggle, J. Bradshaw, Kinetics of the reaction between water and uranium hydride prepared under conditions relevant to uranium storage. *J. Alloys Compd.* **695**, 3727–3735 (2017).
5. S. Imoto, T. Tanabe, K. Utsunomiya, Separation of hydrogen isotopes with uranium hydride. *Int. J. Hydrogen Energy* **7**, 597–601 (1982).
6. J. E. Burke, C. S. Smith, The formation of uranium hydride. *J. Am. Chem. Soc.* **69**, 2500–2502 (1947).
7. R. N. R. Mulford, F. H. Ellinger, W. H. Zachari-Asen, A new form of uranium hydride. *J. Am. Chem. Soc.* **76**, 297–298 (1954).
8. R. E. Rundle, The structure of uranium hydride and deuteride. *J. Am. Chem. Soc.* **69**, 1719–1723 (1947).
9. R. E. Rundle, The hydrogen positions in uranium hydride by neutron diffraction. *J. Am. Chem. Soc.* **73**, 4172–4174 (1951).
10. P. F. Souter, G. P. Kushto, L. Andrews, M. Neurock, Experimental and theoretical evidence for the formation of several uranium hydride molecules. *J. Am. Chem. Soc.* **119**, 1682–1687 (1997).
11. D. Aoki, J. Flouquet, Ferromagnetism and superconductivity in uranium compounds. *J. Phys. Soc. Jpn.* **81**, 011003 (2012).
12. D. Aoki, A. Huxley, E. Ressouche, D. Braithwaite, J. Flouquet, J. P. Brison, E. Lhotel, C. Paulsen, Coexistence of superconductivity and ferromagnetism in URhGe. *Nature* **413**, 613–616 (2001).
13. S. S. Saxena, P. Agarwal, K. Ahilan, F. M. Grosche, R. K. Haselwimmer, M. J. Steiner, E. Pugh, I. R. Walker, S. R. Julian, P. Monthoux, G. G. Lonzarich, A. Huxley, I. Sheikin, D. Braithwaite, J. Flouquet, Superconductivity on the border of itinerant-electron ferromagnetism in UGe_2. *Nature* **406**, 587–592 (2000).
14. A. R. Oganov, C. W. Glass, Crystal structure prediction using *ab initio* evolutionary techniques: Principles and applications. *J. Chem. Phys.* **124**, 244704 (2006).
15. A. O. Lyakhov, A. R. Oganov, H. T. Stokes, Q. Zhu, New developments in evolutionary structure prediction algorithm USPEX. *Comput. Phys. Commun.* **184**, 1172–1182 (2013).
16. A. R. Oganov, A. O. Lyakhov, M. Valle, How evolutionary crystal structure prediction works—and why. *Acc. Chem. Res.* **44**, 227–237 (2011).
17. M. Idiri, T. Le Bihan, S. Heathman, J. Rebizant, Behavior of actinide dioxides under pressure: UO_2 and ThO_2. *Phys. Rev. B* **70**, 014113 (2004).
18. T. Le Bihan, S. Heathman, M. Idiri, G. H. Lander, J. M. Wills, A. C. Lawson, A. Lindbaum, Structural behavior of α-uranium with pressures to 100 GPa. *Phys. Rev. B* **67**, 134102 (2003).
19. D. V. Semenok, A. G. Kvashnin, I. A. Kruglov, A. R. Oganov, Actinium hydrides AcH_{10}, AcH_{12}, and AcH_{16} as high-temperature conventional superconductors. *J. Phys. Chem. Lett.* **9**, 1920–1926 (2018).
20. A. G. Kvashnin, D. V. Semenok, I. A. Kruglov, A. R. Oganov, High-Temperature Superconductivity In Th-H System At Pressure Conditions. arxiv.org/abs/1711.00278 (8 November 2017).
21. J. P. Perdew, K. Burke, M. Ernzerhof, Generalized gradient approximation made simple. *Phys. Rev. Lett.* **77**, 3865–3868 (1996).
22. G. Kresse, D. Joubert, From ultrasoft pseudopotentials to the projector augmented-wave method. *Phys. Rev. B* **59**, 1758–1775 (1999).
23. G. Kresse, J. Furthmüller, Efficient iterative schemes for *ab initio* total-energy calculations using a plane-wave basis set. *Phys. Rev. B* **54**, 11169–11186 (1996).
24. G. Kresse, J. Hafner, *Ab initio* molecular dynamics for liquid metals. *Phys. Rev. B* **47**, 558–561 (1993).
25. G. Kresse, J. Hafner, *Ab initio* molecular-dynamics simulation of the liquid-metal–amorphous-semiconductor transition in germanium. *Phys. Rev. B* **49**, 14251–14269 (1994).
26. C. J. Pickard, R. J. Needs, Structure of phase III of solid hydrogen. *Nat. Phys.* **3**, 473–476 (2007).
27. S. Adak, H. Nakotte, P. F. de Châtel, B. Kiefer, Uranium at high pressure from first principles. *Phys. B Condens. Matter* **406**, 3342–3347 (2011).
28. P. Giannozzi, S. Baroni, N. Bonini, M. Calandra, R. Car, C. Cavazzoni, D. Ceresoli, G. L. Chiarotti, M. Cococcioni, I. Dabo, A. Dal Corso, S. de Gironcoli, S. Fabris, G. Fratesi, R. Gebauer, U. Gerstmann, C. Gougoussis, A. Kokalj, M. Lazzeri, L. Martin-Samos, N. Marzari, F. Mauri, R. Mazzarello, S. Paolini, A. Pasquarello, L. Paulatto, C. Sbraccia, S. Scandolo, G. Sclauzero, A. P. Seitsonen, A. Smogunov, P. Umari, R. M. Wentzcovitch, QUANTUM ESPRESSO: A modular and open-source software project for quantum simulations of materials. *J. Phys. Condens. Matter* **21**, 395502 (2009).
29. S. Baroni, S. de Gironcoli, A. Dal Corso, P. Giannozzi, Phonons and related crystal properties from density-functional perturbation theory. *Rev. Mod. Phys.* **73**, 515–562 (2001).
30. A. Togo, I. Tanaka, First principles phonon calculations in materials science. *Scr. Mater.* **108**, 1–5 (2015).
31. G. M. Eliashberg, Interactions between electrons and lattice vibrations in a superconductor. *J. Exp. Theor. Phys.* **11**, 696–702 (1960).
32. L. P. Gor'kov, On the energy spectrum of superconductors. *J. Exp. Theor. Phys.* **34**, 505–508 (1958).
33. A. B. Migdal, Interaction between electrons and lattice vibrations in a normal metal. *J. Exp. Theor. Phys.* **34**, 996–1001 (1958).
34. E. G. Maksimov, D. Y. Savrasov, S. Y. Savrasov, The electron-phonon interaction and the physical properties of metals. *Physics-Uspekhi* **40**, 337 (1997).
35. P. B. Allen, R. C. Dynes, Transition temperature of strong-coupled superconductors reanalyzed. *Phys. Rev. B* **12**, 905–922 (1975).
36. A. F. Goncharov, V. B. Prakapenka, V. V. Struzhkin, I. Kantor, M. L. Rivers, D. A. Dalton, X-ray diffraction in the pulsed laser heated diamond anvil cell. *Rev. Sci. Instrum.* **81**, 113902 (2010).
37. V. B. Prakapenka, A. Kubo, A. Kuznetsov, A. Laskin, O. Shkurikhin, P. Dera, M. L. Rivers, S. R. Sutton, Advanced flat top laser heating system for high pressure research at GSECARS: Application to the melting behavior of germanium. *High Pressure Res.* **28**, 225–235 (2008).
38. A. E. Karakozov, E. G. Maksimov, A. A. Mikhaĭlovskiĭ. Superconductivity in systems with strong electron–phonon interaction. *J. Exp. Theor. Phys.* **75**, 70–76 (1992).
39. N. A. Kudryashov, A. A. Kutukov, E. A. Mazur. Critical temperature of metallic hydrogen at a pressure of 500 GPa. *J. Exp. Theor. Phys. Lett.* **104**, 460–465 (2016).
40. N. A. Kudryashov, A. A. Kutukov, E. A. Mazur, Critical temperature of metallic sulfur hydride at 225 GPa. *Zh. Eksp. Teor. Fiz.* **151**, 165 (2017).

Acknowledgments

Funding: This work was supported by Russian Science Foundation (grant 16-13-10459). We are very grateful to D. Semenok for fruitful discussions. Portions of this work were performed at GSECARS (The University of Chicago, sector 13), APS, ANL. GSECARS is supported by the

National Science Foundation–Earth Sciences (EAR-1634415) and Department of Energy–GeoSciences (DE-FG02-94ER14466). This research used resources of the APS, a U.S. Department of Energy (DOE) Office of Science User Facility operated for the DOE Office of Science by ANL under contract no. DE-AC02-06CH11357. Financial support from the National Natural Science Foundation of China (nos. 11674330, 11504382, and 11604342) is acknowledged. A.F.G. was supported by the Chinese Academy of Sciences visiting professorship for senior international scientists (grant no. 2011T2J20), Recruitment Program of Foreign Experts and National Natural Science Foundation of China (no. 21473211). Sh. J. acknowledges support of the Chinese Academy of Science (grant no. YZ201524) and a Science Challenge Project no. TZ201601. **Author contributions:** I.A.K., A.V.Y., and A.R.O. designed the study. I.A.K. and A.G.K. performed calculations. A.F.G., S.S.L., N.H., Sh. J., V.B.P., and E.G. performed high-pressure experiments. I.A.K., A.G.K., A.R.O., and A.F.G. wrote the paper. **Competing interests:** The authors declare that they have no competing interests. **Data and materials availability:** All data needed to evaluate the conclusions in the paper are present in the paper and/or the supplementary materials. Additional data related to this paper may be requested from the authors.

Submitted 24 April 2018
Accepted 4 September 2018
Published 12 October 2018
10.1126/sciadv.aat9776

Citation: I. A. Kruglov, A. G. Kvashnin, A. F. Goncharov, A. R. Oganov, S. S. Lobanov, N. Holtgrewe, S. Jiang, V. B. Prakapenka, E. Greenberg, A. V. Yanilkin, Uranium polyhydrides at moderate pressures: Prediction, synthesis, and expected superconductivity. *Sci. Adv.* **4**, eaat9776 (2018).

ScienceAdvances

Uranium polyhydrides at moderate pressures: Prediction, synthesis, and expected superconductivity

Ivan A. Kruglov, Alexander G. Kvashnin, Alexander F. Goncharov, Artem R. Oganov, Sergey S. Lobanov, Nicholas Holtgrewe, Shuqing Jiang, Vitali B. Prakapenka, Eran Greenberg and Alexey V. Yanilkin

Sci Adv **4** (10), eaat9776.
DOI: 10.1126/sciadv.aat9776